To be presented at the Intern.
Conference on Corrosion Fatigue,
Storrs, CT, June 14-18, 1971

UCRL-20538
Preprint c.2

RECEIVED
LAWRENCE
RADIATION LABORATORY

DOCUMENTS SECTION

A SUPERPOSITION MODEL FOR ENVIRONMENTALLY-ASSISTED FATIGUE-CRACK PROPAGATION

W. W. Gerberich, J. P. Birat, and V. F. Zackay

March 1971

AEC Contract No. W-7405-eng-48

TWO-WEEK LOAN COPY

This is a Library Circulating Copy which may be borrowed for two weeks. For a personal retention copy, call Tech. Info. Division, Ext. 5545

LAWRENCE RADIATION LABORATORY
UNIVERSITY of CALIFORNIA BERKELEY

UCRL-20538 c.2

25

DISCLAIMER

This document was prepared as an account of work sponsored by the United States Government. While this document is believed to contain correct information, neither the United States Government nor any agency thereof, nor the Regents of the University of California, nor any of their employees, makes any warranty, express or implied, or assumes any legal responsibility for the accuracy, completeness, or usefulness of any information, apparatus, product, or process disclosed, or represents that its use would not infringe privately owned rights. Reference herein to any specific commercial product, process, or service by its trade name, trademark, manufacturer, or otherwise, does not necessarily constitute or imply its endorsement, recommendation, or favoring by the United States Government or any agency thereof, or the Regents of the University of California. The views and opinions of authors expressed herein do not necessarily state or reflect those of the United States Government or any agency thereof or the Regents of the University of California.

A SUPERPOSITION MODEL FOR ENVIRONMENTALLY-ASSISTED FATIGUE-CRACK PROPAGATION

W. W. Gerberich, J. P. Birat and V. F. Zackay

Inorganic Materials Research Division, Lawrence Radiation Laboratory,
Department of Materials Science and Engineering, College of Engineering
University of California, Berkeley, California

ABSTRACT

An analytical superposition model, which describes fatigue and stress-corrosion-cracking (SCC) components as independent processes, is derived for corrosion fatigue of high strength aluminum and steel alloys. In describing the SCC component, it was desirable to invoke a new parameter, $K_{ISCC(f)}$, which is the threshold stress intensity for environmentally-assisted fatigue crack propagation. In part, this explains how the relative contributions of SCC and fatigue components might change with stress intensity range and ratio of maximum to minimum stress intensity. Experimental data from both aluminum and steel alloys indicate that hydrogen-diffusion models can be utilized as the thermally-activated mechanisms of the SCC components. For example, the activation energy for corrosion fatigue crack propagation in a high-strength metastable austenitic steel was found to be 8500 cal/mol. As long as the SCC mechanism was independent of the stress state (e.g. there may be a fracture morphology change due to a plane strain to plane stress transition), the proposed model could describe the corrosion-fatigue rates within a factor of two.

INTRODUCTION

How to utilize fracture mechanics approaches in designing for relatively simple forms of subcritical crack growth has been aptly pointed out by a number of investigators.[1-3] Unfortunately, different types of subcritical crack growth often operate simultaneously in structural components. Nevertheless, in principle, if two cracking mechanisms such as stress-corrosion cracking (SCC) and fatigue-crack propagation act relatively independent of each other, then it should be feasible to propose a simple superposition model to predict corrosion-fatigue rates. If this were possible, we could then translate our reservoir of knowledge pertaining to fatigue-crack propagation and stress-corrosion cracking to the corrosion-fatigue arena. The present paper is an attempt to present a simple analytical approach to the superposition of these two cracking mechanisms. It should be pointed out that any such direct superposition would necessitate (1) the same SCC fracture mechanism to be operative in both the static and dynamic situations and (2) the same diffusion equations to be involved so that the time-dependent function can be applied to dynamic loadings.

The present model was derived independently of a model proposed earlier by Wei and Landes.[4] This work subsequently came to our attention and it is of some use to point out several similarities and differences in the two approaches. The similarities are strong in that, first, both assume a simple superposition of fatigue and SCC components. Secondly, both assume the two cracking mechanisms to proceed independently without synergistic effects. Finally, both incorporate the integration of the SCC component over the load-time history of a fatigue cycle. The differences are slight but significant. First, Wei and Landes[4] assumed

a sinusoidal load-time variation while we have made a triangular-wave approximation. Secondly, they integrated the SCC growth rate over a single fatigue cycle using a step-wise procedure involving numerical or graphical solutions. We have utilized the mean value theorem to assess the average stress intensity in any one cycle and taken known relationships between SCC growth rate, da/dt, and stress intensity, K, to determine an analytical function for the corrosion-fatigue rate. Finally, while Wei and Landes had incorporated the stress intensity range, K_{min} to K_{max}, as the controlling loading parameter, we have defined the functional dependence to account for the minimum stress intensity of any fatigue cycle being greater or less than a threshold stress intensity level for SCC under fatigue conditions. This later refinement could possibly explain the large variation between theory and experiment noted by Wei and Landes[4] at high K_{min}/K_{max} values.

In the following sections, the proposed theoretical model will be derived for any corrosion-fatigue cycle and then will be evaluated with respect to two material systems. The first will be data on high-strength aluminum alloys from Gerberich, et al.[5] and Feeney, et al.[6] to analyse point (1) above. With respect to point (2), a second set of data were generated during the present investigation to provide unambiguous confirmation of the thermally-activated mechanism involved in the corrosion-fatigue process of high-strength steels.

THEORETICAL MODEL

The proposed model superimposes a fatigue contribution, $(da/dN)_f$, and a stress-corrosion-cracking contribution, $(da/dN)_{SCC}$, to depict corrosion fatigue rates by

$$da/dN = (da/dN)_f + (da/dN)_{SCC} \tag{1}$$

Putting the fatigue contribution in terms of the stress intensity range, ΔK, and assuming the stress corrosion process to be discontinuous in nature, Eq. (1) may be rewritten as

$$da/dN = m(\Delta K)^n + \text{No. of SCC Jumps/cycle} \times \text{Av. Jump Size} \tag{2}$$

For the moment, just consider the SCC component. The number of jumps is simply the time available for jumps divided by the average time between jumps. The former should be some fraction, α, of the reciprocal of cycling frequency, $1/f$, while the latter may be thought of as an average secondary incubation time, Δt_{sAV}. Thus,

$$\text{No. of SCC Jumps/cycle} = \alpha\left(\frac{1}{f\Delta t_{sAV}}\right) \tag{3}$$

The average jump size is taken since at low stress intensity levels the distance the crack might grow per jump may be small compared to high stress intensity levels. As the stress intensity varies over the fatigue cycle, this average jump must be assessed. Taking this as ℓ^*_{AV}, we find from Eqs. (1), (2) and (3) that

$$\begin{aligned} da/dN &= m(\Delta K)^n + \frac{\alpha \ell^*_{AV}}{f\Delta t_{sAV}} \\ &= m(\Delta K)^n + \left(\frac{\alpha}{f}\right)(da/dt)_{AV} \end{aligned} \tag{4}$$

At first glance one might think that α should be unity in all cases. If the minimum stress intensity of the fatigue cycle were very high, then this would probably be true. Or, if SCC occurred under fatigue conditions regardless of the stress intensity level, this would be true. However, if there is a stress intensity level below which there is no environmental effect in fatigue, and if the minimum stress intensity level drops below this threshold, then α is no longer unity.

This, of course, presupposes that there is a threshold stress intensity under fatigue conditions, $K_{ISCC(f)}$. In fact, this was strongly indicated by some data of Feeney, et al.[6] for 2024-T3 aluminum wherein fatigue-crack propagation data obtained in distilled water was considerably greater than that in air except that the curves merged near a ΔK of about 2500 psi-in.$^{1/2}$. For a K_{max}/K_{min} ratio of two, this gives a K_{max} of about 5000 psi-in.$^{1/2}$ and if it is assumed that $K_{ISCC(f)} \sim$ 5000 psi-in.$^{1/2}$, then one can reason that the curves should merge at these low stress intensity levels. Similarly, some data by Wei and Landes[7] on 7075-T651 give a merging of data tested in argon and distilled water near a ΔK of 5000 psi-in.$^{1/2}$, which for the zero to max loading used, would indicate a $K_{ISCC(f)} \sim$ 5000 psi-in.$^{1/2}$. There had been some previous experimental data which indicated there was no relationship between a stress-corrosion-cracking threshold, K_{ISCC}, and corrosion-fatigue rates. For 12 Ni- and 18 Ni-maraging steels, Crooker and Lange[8] had shown that environmental effects in corrosion fatigue persisted at stress intensity levels well below K_{ISCC}. However, there is no <u>a priori</u> reason to believe that the threshold under dynamic loading conditions should be the same as that under static conditions. In fact, there are

persuasive reasons for believing that $K_{ISCC(f)}$ should be less than K_{ISCC}. First, there is a cyclically-reversed plastic zone at the tip of a fatigue crack which should have a higher defect density than a plastic zone that has formed under monotonic loading. This, alone, would have a tendency to make the material more crack-sensitive because of its work-hardened condition.† Secondly, the crack tip could be more chemically active under cyclic conditions due to several surface effects. For example, the reversed plastic zone could provide a greater number of active dissolution sites in the form of emerging dislocations, vacancies or di-vacancies. Furthermore, mechanical breakdown of the oxide layer during opening and closing of the crack or surface exposure resulting from asperities rubbing each other might lead to an enhanced corrosion process. Assuming then that there is a $K_{ISCC(f)} \leq K_{ISCC}$, the following model results:

$K_{min} \geq K_{ISCC(f)}$

This is the simplest case since SCC can occur throughout the fatigue loading cycle. As schematically shown in Fig. 1, the average SCC jump may be given in terms of the mean value theorem by

$$\ell^*_{AV} = \frac{1}{K_{max}-K_{min}} \int_{K_{min}}^{K_{max}} F(K)\, dK \qquad (5)$$

Since $K_{min} \geq K_{ISCC(f)}$, α is unity so that from Eqs. (4) and (5),

---

† For high-strength steels there is an increasing susceptibility to hydrogen embrittlement and SCC with increasing strength level. This strength level effect is discussed in more detail later.

$$(da/dN)_{SCC} = \frac{1}{f(K_{max}-K_{min})} \int_{K_{min}}^{K_{max}} F'(K)\, dK \qquad (6)$$

where F'(K) includes the thermally-activated component which controls Δt_{sAV}. A description of F'(K) was obtained in a separate study[5] of SCC in a 7075-T6 aluminum alloy subjected to a 3.5 percent NaCl solution with $AlCl_3$ added to lower the pH to about two. It was found that the SCC crack growth process was very rapid with growth rates ranging from about 10^{-5} to 10^{-3} in./sec for the stress intensity and test temperature ranges of 20,000 to 50,000 psi-in.$^{1/2}$ and 10° to 73°C. Furthermore, scanning electron microscopy and acoustic emission techniques definitely established the crack growth mechanism to be a combined dissolution and mechanical rupture process. It was also determined that there was a unique activation energy associated with the process that was independent of the stress intensity level and equal to 11,200 ± 1300 cal/mol. Least-square fits to 32 separate data points gave the plots shown in Fig. 2. This activation energy was not too different from that suggested by the data of Tromans and Pathania.[9] Although eight different possible thermally-activated mechanisms were considered,[5] the most likely mechanism involved one of hydrogen diffusion. The activation energy for diffusion of hydrogen in aluminum has been given by Eichenauer and Pebler[10] and Matsuo and Hirata[11] to be 10,900 and 13,000 cal/mol. The activation energy analysis was combined with stress-wave emission and fractographic interpretation of the relative areas consumed by the mechanical and electrochemical processes. This led to a description of SCC crack growth rate as given by[5]

$$da/dt \simeq \left(\frac{K}{K_{ISCC}} - 1\right)^2 \frac{64D_o e^{-Q/RT}}{w} \tag{7}$$

where w is the width of grain exposed to the advancing crack front; D_o is the diffusion constant equal to 0.0324 in.^{2}/sec which is appropriate to the experimental activation energy of 10,900 cal/mol. Equation (7) was considered to be a reasonable model since it described the crack growth rates within a factor of two. However, to obtain a broader perspective of the model, it is of use to integrate Eq. (7) and show time to failure versus initial applied stress intensity. At any particular test temperature, Eq. (7) can be described by

$$da/dt \simeq \frac{C(K-K_{ISCC})^2}{K_{ISCC}^2} \tag{8}$$

where C is a constant for Constant T. For ease of integration, it is convenient to put da in terms of K and for illustrative purposes the infinite plate solution is utilized, which in terms of the applied stress, σ, is

$$K^2 = \sigma^2 \pi a \tag{9}$$

In the case of a statically-applied load, the stress is constant so that differentiation of Eq. (9) gives

$$da = \frac{2KdK}{\sigma^2 \pi} \tag{10}$$

Combining Eqs. (8) and (10), the time to failure, t_f, may be obtained by integrating between the initial stress intensity level, K_o, and some critical stress intensity level, K_f, at which unstable crack growth

occurs, giving

$$\int_{o}^{t_f} dt = \int_{K_o}^{K_f} \frac{2K\, K_{ISCC}^2}{C\sigma^2\pi(K-K_{ISCC})^2}\, dK \tag{11}$$

Integration of Eq. (11) leads to

$$t_f \propto K_{ISCC}^2 \left\{ \ln\left[\frac{K_f-K_{ISCC}}{\left(\frac{K_o}{K_f}\right)K_f-K_{ISCC}}\right] - \frac{K_{ISCC}}{K_f-K_{ISCC}} + \frac{K_{ISCC}}{\left(\frac{K_o}{K_f}\right)K_f-K_{ISCC}} \right\} \tag{12}$$

in terms of K_{ISCC}, K_f and K_o/K_f. Taking K_f as unity, the general form of Eq. (12) is depicted in Fig. 3 for several values of K_{ISCC}/K_f. Although detailed results could not be found to substantiate the general shape of these curves for aluminum alloys, such curves are found for SCC behavior of titanium alloys.[12] Since they are also the form one would generally anticipate for aluminum alloys, it may be assumed that Eq. (7) is a reasonably good representation of the intergranular SCC mechanism in at least one high-strength aluminum alloy.

It is next appropriate to apply this SCC model to the proposed corrosion-fatigue model. As it will be later shown that the general form of Eq. (7) is also applicable to the steel alloy of this investigation, it is sufficient to generally treat the superposition model by using Eq. (7) as F'(K) in Eq. (6). The results are generalized for any type of loading cycle in terms of the stress intensity ratio, β, and the stress intensity range, ΔK, the interrelationships being given by

$$\begin{aligned} \beta &= K_{max}/K_{min};\ K_{max} = \Delta K\left[\frac{\beta}{\beta-1}\right] \\ \Delta K &= K_{max}-K_{min};\ K_{min} = \Delta K\left[\frac{1}{\beta-1}\right] \end{aligned} \tag{13}$$

Combining Eqs. (6), (7) and (13) gives

$$(da/dN)_{SCC} = \frac{64\ D_o e^{-Q/RT}}{fw\Delta K} \int_{\Delta K[\frac{1}{\beta-1}]}^{\Delta K[\frac{\beta}{\beta-1}]} \left(\frac{K-K_{ISCC(f)}}{K_{ISCC(f)}}\right)^2 dK \quad (14)$$

which finally reduces to

$$(da/dN)_{SCC} = \frac{64D_o e^{-Q/RT}}{3fwK^2_{ISCC(f)}} \left[\Delta K^2 \left\{\frac{\beta^2+\beta+1}{(\beta-1)^2}\right\} - 3\Delta K K_{ISCC(f)}\left\{\frac{\beta+1}{\beta-1}\right\} + 3K^2_{ISCC(f)}\right] \quad (15)$$

This predicts a small but significant difference in growth rates as a function of β. For example, if ΔK were 20 times as large as $K_{ISCC(f)}$, for a β of two, the SCC component of the crack growth rate would be 6.5 times as fast as for a β of 20.

What has been considered thus far is that the minimum stress intensity is greater than $K_{ISCC(f)}$ and thus the contribution of the SCC mechanism to the growth process is continuously occurring throughout each fatigue cycle. However, if $K_{ISCC(f)}$ is sufficiently high so that $K_{min} < K_{ISCC(f)}$, it is obvious that at the minimum of the stress intensity range, there should be no SCC contribution for that part of the cycle. Thus, this case must be treated separately.

$K_{min} \leq K_{ISCC(f)}$

From the schematic in Fig. 4, two differences between this and the previous case are immediately noted. First, the proper integration limits for the mean value determination of the average K should be $K_{ISCC(f)}$ to K_{max}. Secondly, the total time of the cycle involved in SCC is α/f as estimated by the triangular wave form in the schematic. Incorporating these two features into Eq. (4) leads to

$$(da/dN)_{SCC} = \frac{1}{f}\left[\frac{K_{max}-K_{ISCC(f)}}{K_{max}-K_{min}}\right]\int_{K_{ISCC(f)}}^{K_{max}} F'(K)\,dK \qquad (16)$$

where the term in bracketts is α. In a similar manner as before, utilization of Eqs. (7), (13) and (16) finally reduces to

$$(da/dN)_{SCC} = \frac{64D_o e^{-Q/RT}}{3fw\,K^2_{ISCC(f)}}\left[\frac{\left\{\Delta K[\frac{\beta}{\beta-1}] - K_{ISCC(f)}\right\}^3}{\Delta K}\right] \qquad (17)$$

One may note that the functional dependence of Eq. (17) is considerably different from Eq. (15) with respect to the major loading variables, ΔK and β, and the material parameter, $K_{ISCC(f)}$. This can be illustrated by taking a ΔK equal to $K_{ISCC(f)}$ so that $K_{min} \leq K_{ISCC(f)}$ and calculating $(da/dN)_{SCC}$. In this case, the SCC component for a β of two would be about 6000 times as large as for a β of 20. A much larger factor shows up in this case than for the one illustrated previously for $K_{min} \geq K_{ISCC(f)}$ because only a very small part of the load cycle is greater than $K_{ISCC(f)}$ for β=20. In reality, many corrosion fatigue curves might have part of their data governed by $K_{min} \leq K_{ISCC(f)}$ and partly by $K_{min} \geq K_{ISCC(f)}$ so that one would have to be careful in making generalizations about how β might affect the crack growth rate.

Combining the appropriate equation for $(da/dN)_{SCC}$ with Eq. (1) allows an analytical prediction of corrosion-fatigue crack growth rates. It should be cautioned here that this analysis is only valid for materials exhibiting a SCC process describable by Eq. (7). Furthermore, the fracture morphology due to the SCC process exhibited under fatigue conditions must be essentially the same as that detected under static

conditions. Finally, this analysis should only be applied to relatively low cyclic frequencies, i.e. < 10 cycles/sec. At much higher frequencies, either synergistic effects of environment and fatigue or localized adiabatic heating would render such a simple analysis invalid. Nevertheless, within the limitations outlined here, it is next of interest to compare this model to some experimental evidence.

EXPERIMENTAL PROGRAM

To test out the general form of the equations with respect to the loading variables, some data by Feeney, et al.[6] on high-strength aluminum alloys in aqueous solutions were available. In several cases the fracture appearances were very similar to those obtained on the high-strength aluminum alloy utilized to develop the SCC analysis. Therefore, direct use of Eqs. (15) and (17) was possible.

It would have been best to analyse the same material or material types with respect to the thermally-activated mechanism. However, no such data could be found. There are some data by Wei[13] at very high cyclic frequencies (143 cycles/sec) on 7075-T651 aluminum in distilled water. However, not only did he find an apparent activation energy that varied with stress intensity level, but he also found that there was a similar apparent activation energy in dry gaseous environments. Partially because of the ambiguous nature of the activation energy in this alloy[†] and partially because we were in the middle of a program evaluating the properties of metastable austenites, we decided to evaluate the thermally-activated mechanism in the later material.

High-strength metastable austenites have been extensively investigated with respect to their strength, ductility and fracture characteristics.[14-18] One unique property is the relatively high toughness that may be achieved due to the transformation of austenite to martensite at the crack tip. A choice of a material undergoing a phase transformation during fatigue-crack propagation would at first seem to

---

[†]At lower cyclic frequencies where synergistic and/or adiabatic heating effects might be less, the activation energy might be less ambiguous.

be an undue complication. However, a previous in-depth study[19] on fatigue-crack propagation in dry environments showed these materials to behave in a typical manner with $da/dN \propto (\Delta K)^n$. Furthermore, these materials have several advantages with respect to an environmental fatigue study. Because of their inherent high toughness under static load conditions, relatively high stress intensities may be applied without instability. At low stress intensity levels, the untempered martensite produced at the tip of a crack is very susceptible to hydrogen embrittlement. Thus, an environmentally-assisted fatigue mechanism could be studied over a large range of stress-intensity factors and test temperatures.

The metastable austenite had been commercially† prepared in the form of 0.1 inch thick sheets from the following composition:

wt.%	C	Mn	Si	Cr	Mo	Ni
	0.27	0.43	0.09	11.95	1.90	7.96

The material was thermomechanically processed by successively:

(1) hammer forging the ingot between 1200 and 1000°C to a plate 2.75 in. thick; hot rolling at 1150°C to a plate thickness of 0.70 in. thick;

(2) solution treating at 1150°C followed by water quenching;

(3) warm-rolling at 390°C to a thickness of 0.1 inch.

These stages were intended, respectively, to break up the cast structure, homogenize the composition and strain harden the austenite to obtain a metastable austenite with yield strength over 200,000 psi.

Standard 8-inch long sheet tensile specimens with a 0.1×0.5×2 inch gage section were evaluated over a range of strain rates from 5×10^{-5} to

†Crucible Steel Corporation

0.167 sec^{-1}. Fracture mechanics tests were conducted with 0.1×3×12 inch single-edge-notch (SEN) specimens loaded in a 300,000 lb. Materials Testing System. A fatigue pre-crack was introduced in air at 5 cycles/sec at a stress intensity level sufficiently low so as to keep $da/dN \leq 10^{-5}$ in./cycle. Crack propagation tests were run at crosshead rates ranging from 5×10^{-5} to 5×10^{-2} in./sec in both distilled-water (pH~4.5) and air environments. In order to make estimates of the plane stress fracture toughness, the observed critical crack length was utilized in the calculation. As discussed elsewhere,[16] this observed critical crack length can be obtained from the macroscopic fracture-mode transition which occurs when the crack starts running at appreciable velocities.

Corrosion-fatigue crack propagation tests were run at 5 cycles/sec in both air and distilled water (pH~4.5) and at 0.07 cycles/sec in distilled water at 0°, 24° and 60°C. Crack growth rates were followed with a measuring microscope in units of about 0.05 inches at both surfaces. For both static and fatigue-crack propagation studies, the stress intensity was calculated from[20]

$$K = Y \frac{P(a)^{1/2}}{B} \tag{18}$$

$$Y = 1.99 - 0.41(a/W) + 18.70(a/W)^2 - 38.48(a/W)^3 + 53.85(a/W)^4$$

where P is the applied load, B is the thickness and W is the width.

RESULTS AND DISCUSSION

Aluminum Data

Since Feeney, et al.[6] conducted their experimental tests at a β of two, Eqs. (15) and (17) were reduced accordingly and in conjunction with Eq. (1) gave

$$\frac{da}{dN} = m(\Delta K)^n + \frac{64D_o e^{-Q/RT}}{fw} \times \left[\frac{8(\Delta K)^3 - 12(\Delta K)^2 K_{ISCC(f)} + 6\Delta K\, K^2_{ISCC(f)} - K^3_{ISCC}}{\Delta K \cdot 3K^2_{ISCC(f)}}\right] \quad \text{for } K_{min} \leq K_{ISCC(f)}$$

$$\frac{da}{dN} = m(\Delta K)^n + 64D_o e^{-Q/RT} \times \left[\frac{7(\Delta K)^2 - 9(\Delta K)K_{ISCC(f)} + 3K^2_{ISCC(f)}}{3K^2_{ISCC(f)}}\right] \quad \text{for } K_{min} \geq K_{ISCC(f)} \tag{19}$$

One can demonstrate that these two equations are equivalent at $K_{min} = K_{ISCC(f)}$ as they should be. A reasonable log-log relationship for their data tested in air gave m and n and the diffusivity values were taken for the activation energy closest to that observed in the SCC study.[5] The value for the grain width, w, was estimated from micrographs published by Feeney, et al.[6] to be about 5μ for both 2024-T3 and 7178-T6 data. They also investigated 7075-T6 aluminum but this was not considered here since no intergranular fracture was observed on the corrosion-fatigue fracture surfaces. The values appropriate to 2024-T3 aluminum are:

$m = 2.9\times10^{-21}$ (in./cycle)(ksi-in.$^{1/2}$)$^{-n}$ $\qquad$ $f = 2$ cycles/sec

$n = 4$ $\qquad$ $w \simeq 5\mu \simeq 2\times10^{-4}$ in.

$D_o = 0.0324$ in.^{2}/sec $\qquad$ $T = 294°K$

$Q = 10{,}900$ cal/mol $\qquad$ $K_{ISCC(f)} \simeq 4.5$ ksi-in.$^{1/2}$ (4500 psi-in.$^{1/2}$)

The only assumption made here is that $K_{ISCC(f)} \simeq 4500$ psi-in.$^{1/2}$ but from the discussion above this would appear to be a reasonable value. Utilizing the above values in Eq. (19) allowed determination of da/dN versus ΔK. Note that for β=2, there is a crossover from the $K_{min} \leq K_{ISCC(f)}$ to the $K_{min} \geq K_{ISCC(f)}$ criterion at ΔK = 4500 psi-in.$^{1/2}$. As shown in Fig. 5, the agreement does not seem particularly good much above a ΔK over 4000 psi-in.$^{1/2}$. However, as discussed by Feeney, et al.,[6] there may be good reason for this. Because of the relatively low yield strength of 2024-T3 as compared to other high-strength aluminum alloys, there is a plane-strain transition which starts near a ΔK value of 5800 psi-in.$^{1/2}$. Coincident with this is the fact that, at stress intensity levels below this transition, intergranular fracture was the major fracture mode while at values much greater than this, ductile fatigue striations predominated. Thus, the reason there is such a large difference between theory and experimental data is that the SCC mechanism has become less severe at higher stress intensity levels. One must ask why this relaxation of plane strain conditions results in a lessening of the environmental attack.

If one does accept the hydrogen mechanism used in this model and espoused by Wei,[13] Hartman,[21] Bradshaw and Wheeler,[22] and Broom and Nichloson,[23] then one can hypothesize that the effect is due to a decreased level of hydrogen per unit crack extension. This could arise if the potential gradient of the stress field acting as a driving force for hydrogen diffusion is lessened as the specimen transcends from a plane strain to a plane stress situation. In a separate study, St. John and Gerberich[24] have shown that the equilibrium solution of the field

equations for interstitials being driven by a potential stress gradient results in

$$C_{eq.} = \frac{C_o e^{\sigma_{ys}[pcf-1/2]V/3kT}}{1 - C_o + C_o e^{\sigma_{ys}[pcf-1/2]V/3kT}} \qquad (20)$$

where C_o is the initial concentration, $C_{eq.}$ is the equilibrium concentration, σ_{ys} is the yield strength, pcf is the plastic constraint factor and V is the partial molal volume of the interstitial in solid solution. Obviously, the present situation is probably not representative of equilibrium conditions. Nevertheless, this gives one the distinct impression that the lower the yield stress, the less potentially severe a hydrogen embrittlement mechanism should be. Also, the lower the plastic constraint factor, as in the case of plane stress, the less severe the embrittlement mechanism should be. Thus, the deviation noted in Fig. 5 has some theoretical basis if hydrogen diffusion is a necessary ingredient to the fracture mechanism.

Next, consider the 7178-T6 aluminum alloy. Here, all parameters are the same as above except that $m \simeq 1.14\times10^{-21}$ and $n \simeq 4.2$. A similar calculation based upon Eq. (19) gives excellent agreement between theory and experiment in Fig. 6. For this material there was no relaxation of plane strain conditions due to the relatively high yield strength of 79,100 psi as compared to 45,700 psi for 2024-T3 aluminum. This was also reflected in the fractographic observations where intergranular fracture predominated in the 3.5 percent NaCl solution at high ΔK levels. Thus, as long as the same SCC embrittlement mechanism predominated, Eq. (19) provided good agreement between theory and experiment. One interesting point about both Figs. 5 and 6 is that as the stress intensity maximum

approaches $K_{ISCC(f)}$ and hence, the SCC component becomes very small, the slope of the da/dN versus ΔK becomes very gradual. Thus, it would appear that very high exponents on ΔK are representative of a transition from a low stress intensity where environmental effects are small to a higher stress intensity where environmental effects predominate.

Metastable Austenitic Steel Data

Before considering the corrosion fatigue data, it is first appropriate to briefly review the uniaxial and fracture characteristics of this alloy. As can be seen in Table 1, increasing strain rate gives a slight increase in upper yield strength and a somewhat greater decrease in elongation. The yield strength effect may be due to the normal dependency of austenite flow stress on strain rate while the elongation effect is definitely an adiabatic heating effect. This later effect comes about when the adiabatic heating at high strain rates raises the temperature sufficiently so that there is a reduced amount of strain-induced phase transformation. The reduced amount of transformation lowers the work-hardening rate which may lead to premature necking as suggested by Gerberich, et al.[15]

With respect to the fracture toughness data, the apparent values listed in Table 2 are very high being on the order of 400,000 psi-in.$^{1/2}$. Keeping in mind that these evaluations were made on 3-inch wide plates, one can only treat this value qualitatively. However, no plastic zone size correction was made to obtain these values so, if anything, 400,000 psi-in.$^{1/2}$ might tend to be conservative. As noted in Table 2, there also appears to be a crosshead rate effect on fracture toughness, an effect that has been attributed to adiabatic heating in a separate analysis of similar steels.[17] Since both flow and fracture properties seemed to be affected

by an adiabatic heating effect, it was of interest to ascertain if the corrosion-fatigue tests might also exhibit such an effect. This is discussed in some detail in the Appendix where it is indicated that there is a likely effect at 5 cycles/sec but not at 0.07 cycles/sec. Since the bulk of the data and the activation energy analysis was performed at 0.07 cycles/sec, we will assume adiabatic heating effects to be of secondary importance.

At 5 cycles/sec the effect of a distilled water environment on fatigue-crack propagation rates is seen to be small in Fig. 7. At most, there is a factor of two difference in the crack growth rate which is barely significant considering the scatter involved. In contrast to this, there was almost an order of magnitude increase in crack growth rate at 0.07 cycles/sec. Additional tests at 0° and 60°C gave the results shown in Fig. 8. It was desirable to utilize this data to make an estimate of the activation energy of the process. However, before this could be done, a model must be invoked. If a simple superposition model as suggested herein is invoked, then just log $(da/dN)_{SCC}$ should be plotted versus 1/T in the Arrhenius analysis. Subtracting out the da/dN component appropriate for the air environment in Fig. 7 from the total values given in Fig. 8 gives the Arrhenius plot in Fig. 9 for two stress intensity levels. It is seen that the activation energy is relatively independent of stress intensity and equal in magnitude to the values reported by Johnson[25] as characteristic of either hydrogen diffusion or hydrogen-embrittlement mechanisms in high-strength martensitic steel. He reported values ranging from 8500-9800 cal/mol with the value for electrolytic diffusion of hydrogen in AISI 4340 steel being 9200 cal/mol.

One may note that this is the activation energy for hydrogen diffusion in the bcc phase while the majority of the material outside the crack-tip region in the present steel is austenitic (fcc). It had been previously shown[18] that hydrogen embrittlement would not proceed in these metastable austenitic steels under static load. This was verified with pre-cracked samples that were charged electrolytically and with samples held in distilled water. Presumably, because of the very slow hydrogen diffusion rates in austenite, a critical hydrogen concentration could never be achieved to propagate the crack. With the cyclic loads, however, there is a continuous production of fresh martensite at the tip of the crack which provides an easy diffusion path for the hydrogen. Thus, at least in this material, one can state unequivocally that $K_{ISCC(f)} << K_{ISCC}$.

Before applying the proposed theoretical model to this data, slight modification of the original derivation is necessary since one would not expect a SCC mechanism derived for high-strength aluminum to apply to steels. The same general approach is utilized and it is assumed that Eq. (4) is also valid here. In fact, for other high-strength steels, the discontinuous jump process has been invoked.[26] Here, it was shown that the crack jump could be approximately related to the crack-tip displacement by

$$\ell^* = \frac{2V_c}{\pi\varepsilon_f} = \frac{K^2}{2\pi\sigma_{ys}E\varepsilon_f} \tag{21}$$

where ε_f is the fracture strain. One slight modification is made to account for a stress intensity threshold which for fatigue conditions gives

$$\ell^* = \frac{\left[K-K_{ISCC(f)}\right]^2}{2\pi\sigma_{ys}E\varepsilon_f} \tag{22}$$

The secondary incubation time is also taken from the hydrogen embrittlement analysis[22] which, as a first approximation, is

$$\Delta t_s \simeq \gamma \frac{d^2}{D} \tag{23}$$

where d is the cleavage facet size, D is the hydrogen diffusivity and γ is a constant. The value of γ is near 10 for the average secondary incubation time if distilled water data are compared to an equivalent crack growth rate for hydrogen embrittlement.† Since d is about 4μ in the present case, one would expect γd^2 to be about 25×10^{-8} in.^{2}. For the diffusivity, if one assumes a room temperature diffusivity of about 2×10^{-7} cm^2/sec,[26] using an activation energy of 8500 cal/mol results in a calculated value of 0.05 in.^{2}/ sec for D_o. With these modifications to the crack step and thermally-activated components, the equation for corrosion fatigue may be obtained as before. The stress intensity dependence is the same as that given by Eq. (17) since the load cycle was zero to maximum giving $K_{min} < K_{ISCC(f)}$ and $\beta=\infty$. Incorporating Eqs. (22) and (23) into (4) and (17) lead to

$$da/dN = m(\Delta K)^n + \frac{D_o e^{-Q/RT}}{f\gamma d^2} \frac{}{2\pi\sigma_{ys} E\varepsilon_f} \left[\frac{(\Delta K - K_{ISCC(f)})^3}{3\Delta K}\right] \tag{24}$$

All parameters have been described except m and n which may be taken from the air environment data in Fig. 7; ε_f which may be approximated as about 0.1 for untempered martensite and $K_{ISCC(f)}$. Although the value

---

†This is somewhat of an oversimplification since it was observed previously that Δt_s was not constant with stress intensity for specimens tested in distilled water but was for electrolytically-charges specimens.[26] Nevertheless, since Δt_s is averaged over the whole fatigue cycle, a value that is approximately equivalent to the hydrogen-embrittlement case for the same stress intensity range is a reasonable estimate.

for $K_{ISCC(f)}$ is somewhat arbitrary, an upper bound is 28,000 psi-in.$^{1/2}$ since an environmental effect was observed at this level in Fig. 8. Also, K_{ISCC} for a very susceptible tempered-martensitic steel, H-11, was reported to be 11,000 psi-in.$^{1/2}$.[25] Thus, as a first approximation a $K_{ISCC(f)}$ of 10,000 psi-in.$^{1/2}$ may be reasonable. As a confirmation of the values chosen, one known value of da/dN = 4.3×10^{-3} in./cycle was taken from Fig. 8 for a ΔK of 100,000 psi-in.$^{1/2}$ and a temperature of 60°C. From Eq. (24) this gave a calculated value for γd^2 of 28.9×10^{-8} in.^{2} which is in good agreement with the original estimate above. Thus, Eq. (24) was utilized with:

$m = 2\times10^{-20}$ (in./cycle)(ksi-in.$^{1/2}$)$^{-n}$	$f = 0.07$ cycles/sec
$n = 3$	$\varepsilon_f = 0.1$
$D_o = 0.05$ in.^{2}/sec	$\gamma d^2 = 28.9\times10^{-8}$ in.^{2}
$Q = 8500$ cal/mol	$\sigma_{ys} = 215{,}000$ psi
	$K_{ISCC(f)} = 10$ ksi-in.$^{1/2}$ (10,000 psi-in.$^{1/2}$)

As is seen in Fig. 10, this superposition model fits the experimental data very well with all data points being within a factor of two of the theoretical estimates. Additional tests are in order to verify the appropriate value for $K_{ISCC(f)}$ and the proposed variation with K_{max}/K_{min}. Nevertheless, the proposed model appears to be a reasonable analytical approach to the corrosion-fatigue problem. Once again, one may note that as $K_{ISCC(f)}$ is approached, the slope of the da/dN versus ΔK curve achieves a very gradual slope which might be represented by some very high exponent on ΔK. Although this trend is not particularly obvious from this data, it is clearly shown by Dahlberg[27] on 4340 steel tested

in humidified air. Here, it appeared that there was a $K_{ISCC(f)}$ near 15,000 to 20,000 psi-in.$^{1/2}$ Whereas the slope in dry air was about three at a stress intensity of 20,000 psi-in.$^{1/2}$, the slope in humidified air was closer to seven. This is just about the difference in slopes observed for the theoretical dry air and distilled water curves shown in Fig. 10 at the lower stress intensity levels for 24°C tests. One further comment about $K_{ISCC(f)}$ is that because of the diffusional nature of the SCC component, there is probably a minimum time involved to build up concentration to a critical level. As this time would be dependent upon frequency, temperature and environment, one must conclude that $K_{ISCC(f)}$ is probably a function of these variables.

CONCLUSIONS

1. An analytical superposition model based upon the mean value theorem for estimating stress intensity effects appears to describe corrosion-fatigue behavior in several high-strength aluminum and steel alloys.

2. Any theoretical model should include the effects of stress intensity range, ratio of maximum to minimum stress intensity, the cyclic frequency, a threshold stress intensity and the thermally-activated mechanism.

3. A threshold stress intensity value for environmentally-assisted fatigue crack propagation, $K_{ISCC(f)}$, is proposed, below which there is no contribution of the environment to fatigue-crack propagation. At the present time it is not known how this threshold value would vary with temperature, cycling frequency and environment.

4. The very high exponents observed when corrosion-fatigue data are plotted as $da/dN \propto (\Delta K)^n$ may be attributed to a transition between a point below $K_{ISCC(f)}$ where the fatigue component controls crack propagation to a point above $K_{ISCC(f)}$ where the stress-corrosion component controls crack propagation.

5. The activation energy for corrosion-fatigue crack propagation in a high-strength metastable austenitic steel is found to be about 8500 cal/mol.

6. For both high strength aluminum and steel alloys, hydrogen-diffusion models can be invoked as the thermally-activated mechanism in corrosion fatigue.

7. The possibility of adiabatic heating effects should be carefully assessed when analysing corrosion-fatigue data at high cycling rates.

ACKNOWLEDGEMENTS

This work was supported by the United States Atomic Energy Commission. The authors would like to thank W. Wood for previously unpublished data on 7075-T6 aluminum and D. Krieger for assistance on mechanical testing.

APPENDIX

An order of magnitude calculation was made to see if the two different cycling frequencies used in the present program could result in a severe strain rate effect. In order to estimate the strain rate at the tip of a crack undergoing corrosion fatigue, a linear elastic analysis is suitable since the plastic zone is small. In terms of a stress intensity factor, the elastic strain distribution is

$$\varepsilon_{yy} = \frac{K}{E[2\pi r]^{1/2}} \qquad \text{(A-1)}$$

where r is the distance in front of the crack along the ray, $\theta=0°$. As suggested by some corrosion-fatigue[28] and hydrogen embrittlement analyses,[26] the region of interest might be the crack-tip displacement, so that there may be a critical strain rate, $d\varepsilon^*_{yy}/dt$, associated with a critical region, r^*, as given by the crack tip displacement†

$$r^* = \frac{K^2_{max}}{2(2\sigma_{ys})E} \qquad \text{(A-2)}$$

where K_{max} is the maximum stress intensity of the fatigue cycle. Combining Eqs. (A-1) and (A-2), differentiating with respect to time and using the infinite plate estimate of $K_{max}=\sigma_{max}[\pi a]^{1/2}$ leads to

$$\frac{d\varepsilon^*_{yy}}{dt} = \left[\frac{1}{a}\frac{da}{dt} + \frac{2}{\sigma_{max}}\frac{d\sigma}{dt}\right]\left[\frac{\sigma_{ys}}{2\pi E}\right]^{1/2} \qquad \text{(A-3)}$$

Taking a typical corrosion-fatigue growth rate of 10^{-4} in./cycle, this would take a maximum stress intensity factor of about 60,000 psi-in.$^{1/2}$ which could be represented by infinite plate parameters of σ_{max}~50,000 psi and a~0.5 inch. Even if the crack growth in a corrosion fatigue cycle

† Note here that there is a factor of 2 magnification on the yield strength in the denominator due to the fatigue loading.

only took 1/100 of the total rise time involved, it may be shown that the resulting da/dt is still too slow to make the first term in Eq. (A-3) significant. Thus, a good approximation is

$$\frac{d\varepsilon^*_{yy}}{dt} \simeq \left[\frac{1}{\sigma_{max}} \frac{d\sigma}{dt}\right]\left[\frac{2\sigma_{ys}}{\pi E}\right]^{1/2} \qquad \text{(A-4)}$$

For the two cyclic frequencies of 5 and 0.07 cycles/sec, a triangular wave approximation gives effective stress rates of 500,000 psi/sec and 7000 psi-sec. For a 200,000 psi yield strength and an applied stress of 50,000 psi, these two stress rates give strain rates of about 0.7 and 0.001 sec^{-1}. These are right in the strain-rate transition region where adiabatic heating has an effect on the elongation characteristics. Of course, the heat-flow conditions at the tip of a crack are not the same as those in a uniaxial tensile test. A more realistic comparison would be to examine the fracture toughness data. In a separate study,[17] it has been shown that the effects indicated in Table 2 may be attributed to adiabatic heating. To obtain an estimate of the strain rate at the tips of these cracks requires a different analysis because of the monotonic loading, the large fracture toughness and the fact that $d\sigma/dt \sim 0$ at instability. Using a plastic strain distribution[29] for the large plastic zones involved and assuming that $\frac{d\sigma}{dt} \sim 0$, one may show that

$$\frac{d\varepsilon^*_{yy}}{dt} \simeq \frac{1}{\pi a} \frac{da}{dt} \qquad \text{(A-5)}$$

Using observed crack velocities and critical crack lengths gives strain rates varying from about 0.06 to 1.3 sec^{-1} for the crosshead variation of 0.0005 to 0.05 in./sec given in Table 2. These values overlap the 0.7 sec^{-1} strain rate estimated for a 5 cycle/sec frequency but not the

0.001 sec^{-1} strain rate estimated for 0.07 cycle/sec frequency. Keeping in mind the order of magnitude estimate involved here, one must conclude that the cyclic frequencies involved in the present study could have an inherent adiabatic heating effect, particularly at 5 cycles/sec.

REFERENCES

1. C. F. Tiffany and J. N. Masters, Fracture Toughness Testing and Its Applications, ASTM STP 381, Am. Soc. Testing Mats., 249 (1965).
2. P. C. Paris and F. Erdogan, J. Basic Eng., 85, 528 (1963).
3. R. P. Wei, Fundamental Aspects of Stress Corrosion Cracking, ed. by Staehle, Forty and Van Rooyen, Nat. Assoc. Corrosion Eng. Houston, 104 (1969).
4. R. P. Wei and J. D. Landes, Mat'ls. Res. and Stds., 9, No. 7, 25 (1969).
5. W. W. Gerberich, W. A. Wood and E. R. Parker, unpublished data to be submitted for publication.
6. J. A. Feeney, J. C. McMillan and R. P. Wei, Met. Trans., 1, 1741 (1970).
7. R. P. Wei and J. D. Landes, Int. J. of Fract. Mech., 5, No. 1, 69 (1969).
8. T. W. Crooker and E. A. Lange, Effects of Environment and Complex Load History on Fatigue Life, ASTM STP 462, Am. Soc. for Test. Mat'ls., 258 (1970).
9. D. Tromans and R. S. Pathania, Extended Abstracts, Fall Meeting of Electrochemical Society, 179 (October 1969).
10. W. Eichenauer and A. Pebler, Z. Metallk., 48, 373 (1957).
11. S. Matsuo and T. Hirata, J. Japan Inst. Metals, 31, No. 4, 590 (1967).
12. D. N. Fager and W. F. Spurr, Trans. Quart. ASM, 61, No. 2, 283 (1968).
13. R. P. Wei, Int. J. Fract. Mech., 4, No. 2, 159 (1968).
14. V. F. Zackay, E. R. Parker, D. Fahr and R. Busch, Trans. Quart. ASM, 60, No. 2, 252 (1967).
15. W. W. Gerberich, G. Thomas, E. R. Parker, and V. F. Zackay, 2nd Int. Conf. on Strength of Metals and Alloys, Vol. III, Asilomar ASM, 894 (1970).

16. W. W. Gerberich, P. L. Hemmings, V. F. Zackay and E. R. Parker, Fracture 1969, ed. by P. L. Pratt, Chapman and Hall, Ltd., London, 288 (1969).

17. W. W. Gerberich, P. L. Hemmings and V. F. Zackay, to be published Met. Trans.

18. R. A. McCoy, W. W. Gerberich and V. F. Zackay, Met. Trans., 1, 2031 (1970).

19. G. Chanani, "Fracture Characteristics of Metastable Austenitic Steels Under Cyclic Loading," Ph. D. Thesis, Univ. of Calif., Berkeley (1970).

20. W. F. Brown, Jr. and J. E. Srawley, Plane Strain Crack Toughness Testing of High Strength Metallic Materials, ASTM STP 410, Philadelphia (1966).

21. A. Hartman, Int. J. Fract. Mech., 1, No. 3, 167 (1965).

22. F. J. Bradshaw and C. Wheeler, Appl. Mat'ls. Res., 5, 112 (1966).

23. T. Broom and A. J. Nicholson, J. Inst. Metals, 89, 183 (1960).

24. C. St. John and W. W. Gerberich, unpublished data.

25. H. H. Johnson, Fundamental Aspects of Stress Corrosion Cracking, ed. by Staehle, Forty and Van Rooyen, Nat. Assoc. Corrosion Eng., Houston, 439 (1969).

26. W. W. Gerberich and C. E. Hartbower, ibid. 420 (1969).

27. E. P. Dahlberg, Trans. ASM, 58, 46 (1965).

28. R. M. N. Pelloux, Fracture 1969, ed. by P. L. Pratt, Chapman and Hall, Ltd., London, 731 (1969).

29. W. W. Gerberich, Experimental Mech., 335, November (1964).

Table 1. Tensile Properties

Strain rate sec^{-1}	Upper Yield (psi)	Lower Yield (psi)	Tensile Strength (psi)	Elongation (%)
0.00005	208,800	201,100	235,500	47.8
0.000167	211,800	202,000	235,800	46.6
0.00067	209,800	193,100	226,600	35.0
0.00167	209,800	199,300	212,700	27.8
0.0042	216,400	204,800	218,100	26.7
0.0167	212,800	202,700	221,800	30.8
0.0167	212,800	204,500	212,800	22.2
0.167	221,000	206,500	221,000	23.9

Table 2. Fracture toughness data.

	Water			Air		
Crosshead Rate (in./sec)	Critical Crack Length (in.)	Critical Load (lbs.)	Fracture Toughness (psi-in.$^{1/2}$)	Critical Crack Length (in.)	Critical Load (lbs.)	Fracture Toughness (psi-in.$^{1/2}$)
0.00005	no instability			no instability		
0.0005	1.69	17,500	480,000	no instability		
0.00167	1.55	17,500	392,000	no instability		
0.005	1.36	15,500	266,000	no instability		
0.05	1.55	16,600	371,000	1.55	18,000	402,000

FIGURE CAPTIONS

1. Schematic of load cycle pertinent to $K_{min} > K_{ISCC(f)}$.
2. Activation energy for SCC in 7075-T6 aluminum.
3. Schematic of time to failure as a function of stress intensity variables for SCC model.
4. Schematic of load cycle pertinent to $K_{min} < K_{ISCC(f)}$.
5. Comparison of corrosion-fatigue model to experiment for 2024-T3 aluminum data from Feeney, et al.[6]
6. Comparison of corrosion-fatigue model to experiment for 7178-T6 aluminum data from Feeney, et al.[6]
7. Effect of environment on crack growth rate of a metastable-austenitic steel tested at 5 cycles/sec.
8. Effect of temperature on crack growth rate of a metastable-austenitic steel tested at 0.07 cycles/sec in distilled water.
9. Arrhenius plot to determine activation energy of thermally-activated component in corrosion fatigue of a metastable-austenitic steel.
10. Comparison of corrosion-fatigue model to experiment for a high-strength metastable austenitic steel.

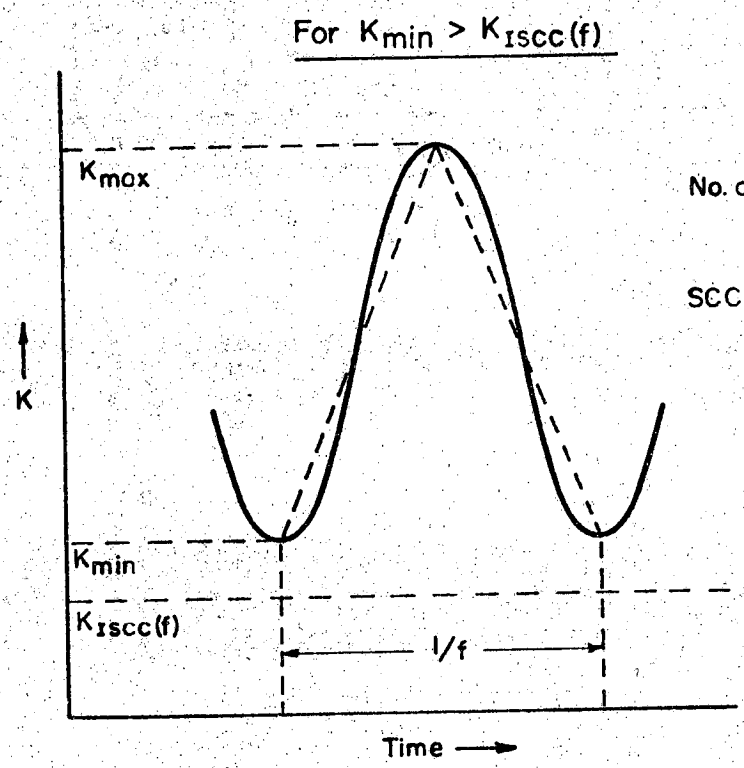

No. of SCC Jumps per Cycle = $\frac{1}{f \Delta t_s}$

SCC Jump = $\frac{1}{K_{max} - K_{min}} \int_{K_{min}}^{K_{max}} F(K)\, dK$

XBL713-6580

Fig. 1.

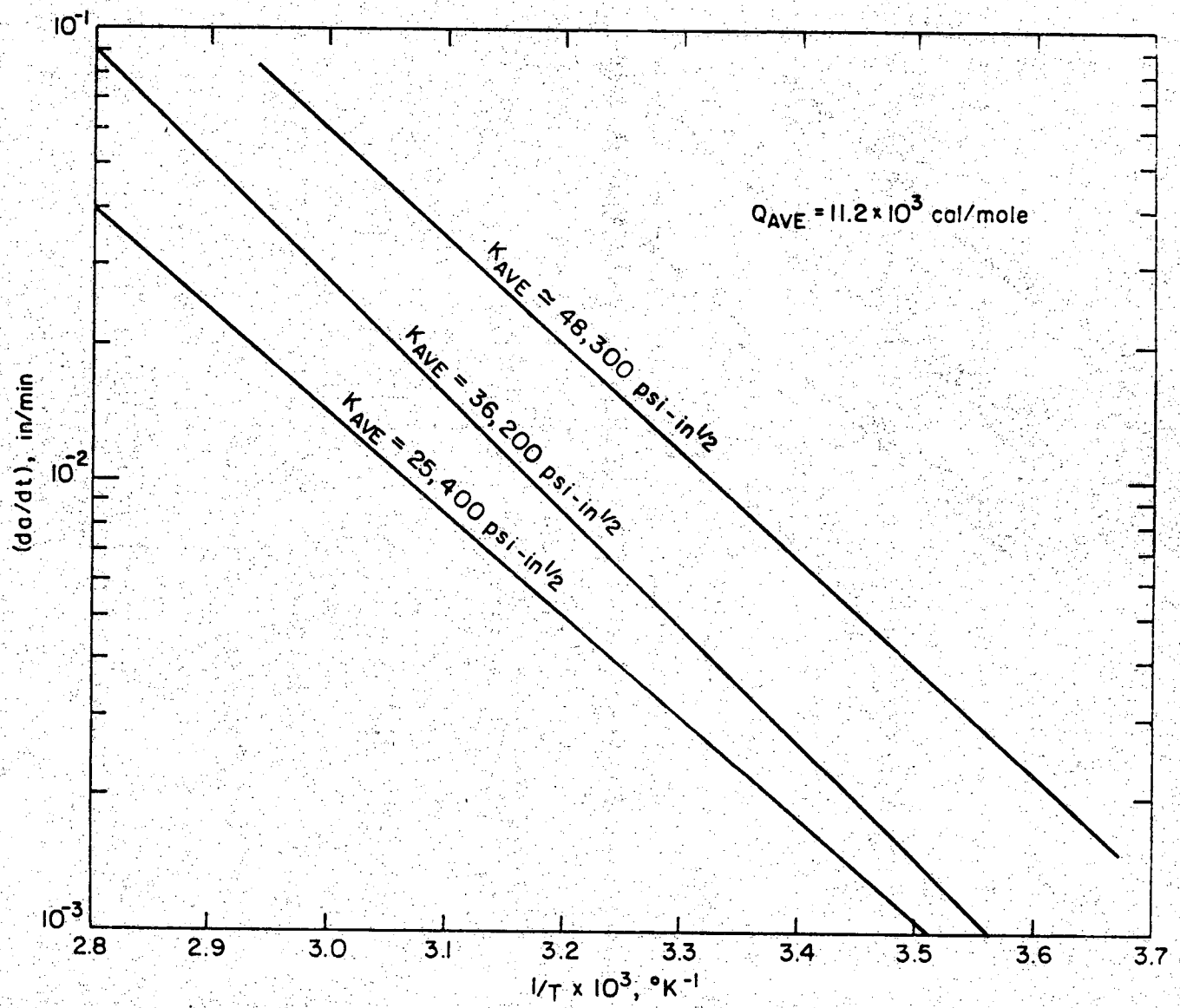

XBL 703-6417

Fig. 2.

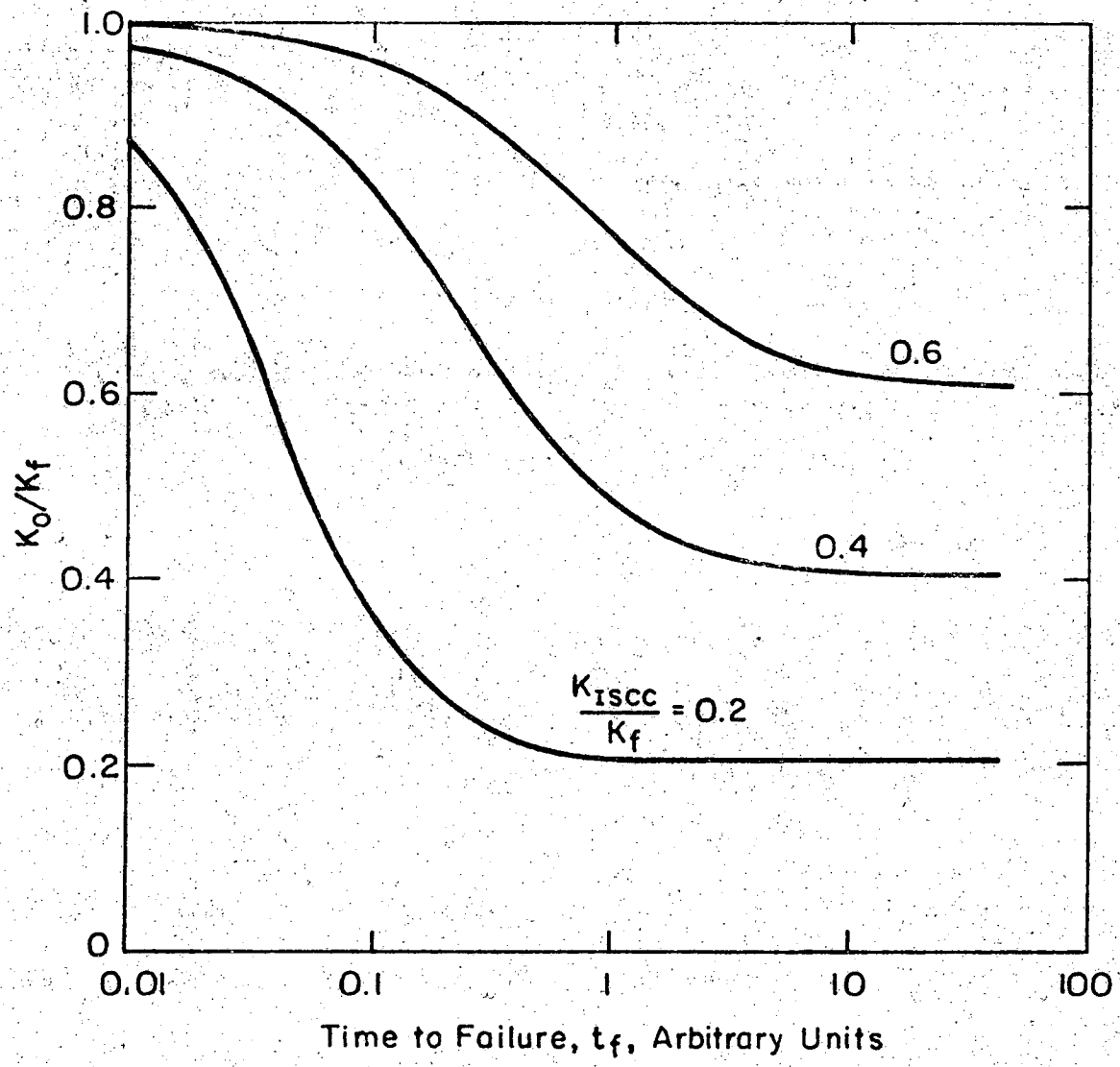

XBL713-6573

Fig. 3.

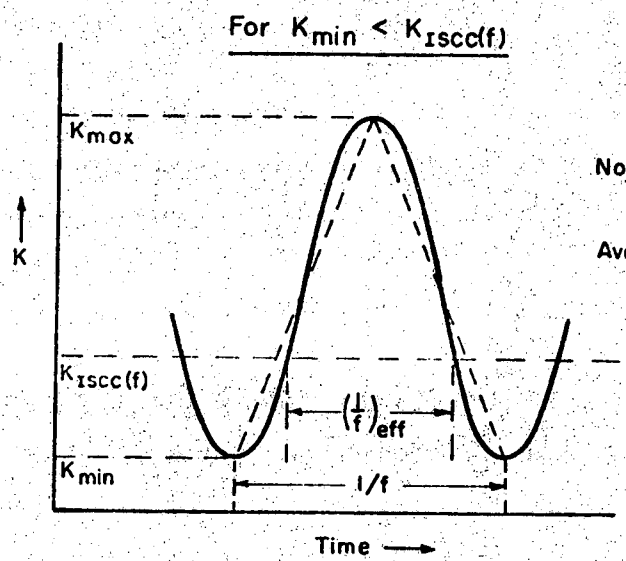

$$\text{No. of SCC Jumps per Cycle} = \left[\frac{K_{max}-K_{Iscc}}{K_{max}-K_{min}}\right]\frac{1}{f\Delta t_s}$$

$$\text{Average SCC Jump} = \frac{1}{K_{max}-K_{Iscc}}\int_{K_{Iscc}}^{K_{max}} F(K)\,dK$$

XBL713-6581

Fig. 4.

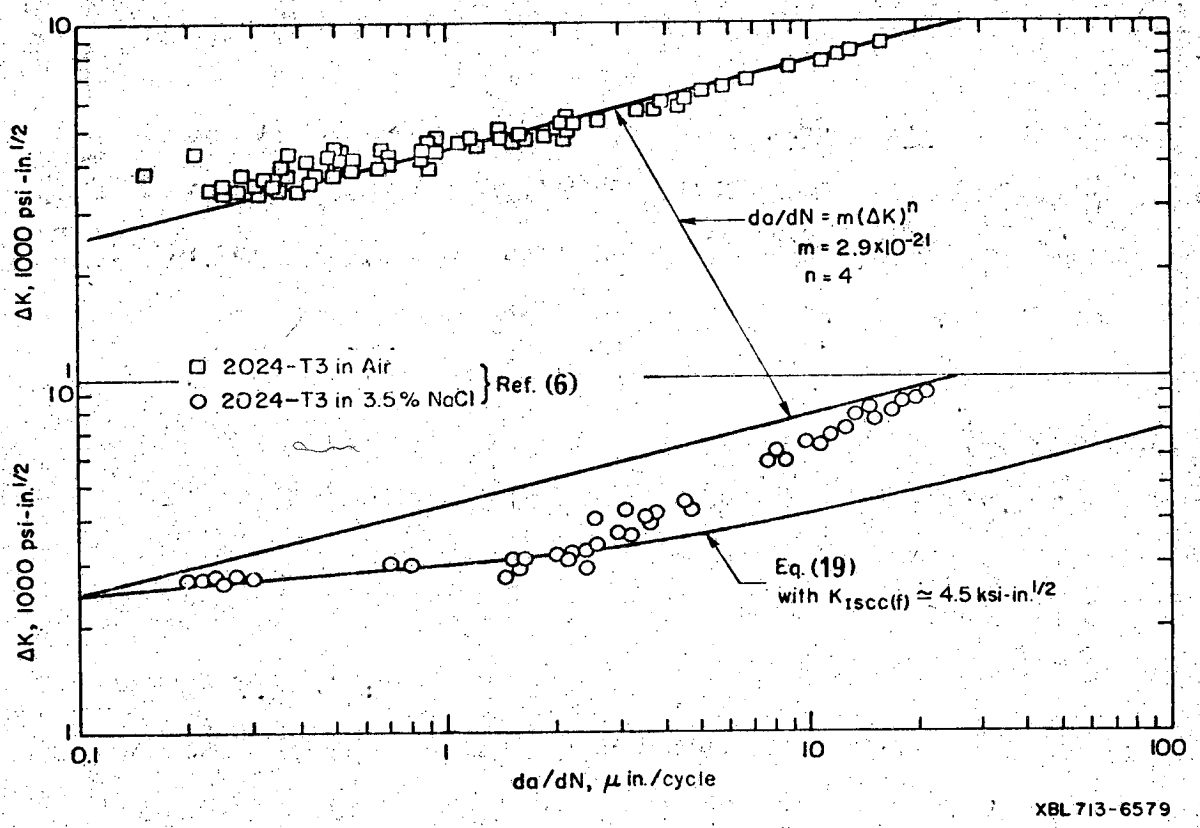
10
1
10
1
ΔK, 1000 psi-in.^1/2
ΔK, 1000 psi-in.^1/2
da/dN = m(ΔK)^n
m = 2.9x10^-21
n = 4
2024-T3 in Air
2024-T3 in 3.5% NaCl
Ref. (6)
Eq. (19)
with K_Iscc(f) ≃ 4.5 ksi-in.^1/2
0.1
1
10
100
da/dN, μ in./cycle
XBL 713-6579

Fig. 5.

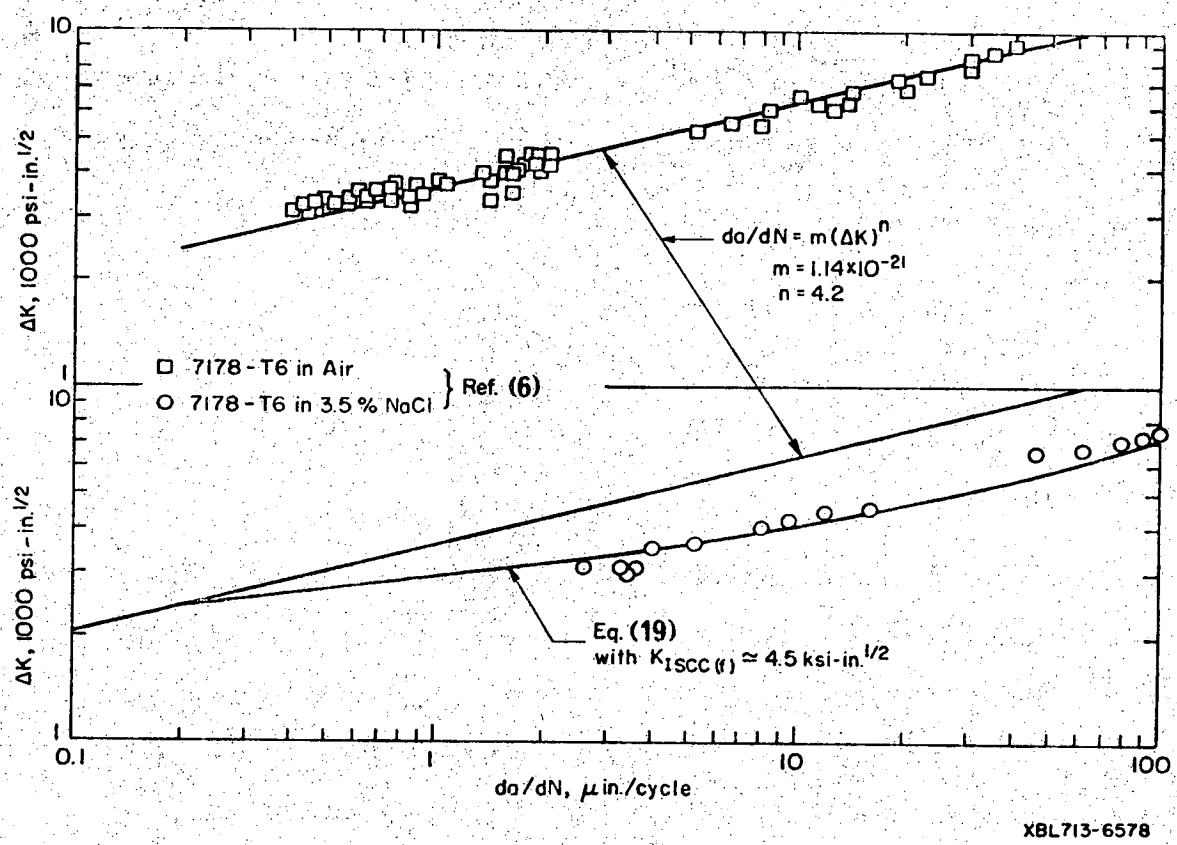
10
1
10
1
ΔK, 1000 psi-in.^1/2
ΔK, 1000 psi-in.^1/2
da/dN = m(ΔK)^n
m = 1.14x10^-21
n = 4.2
7178-T6 in Air
7178-T6 in 3.5% NaCl
Ref. (6)
Eq. (19)
with K_ISCC(f) ≃ 4.5 ksi-in.^1/2
0.1
1
10
100
da/dN, μin./cycle
XBL713-6578

Fig. 6.

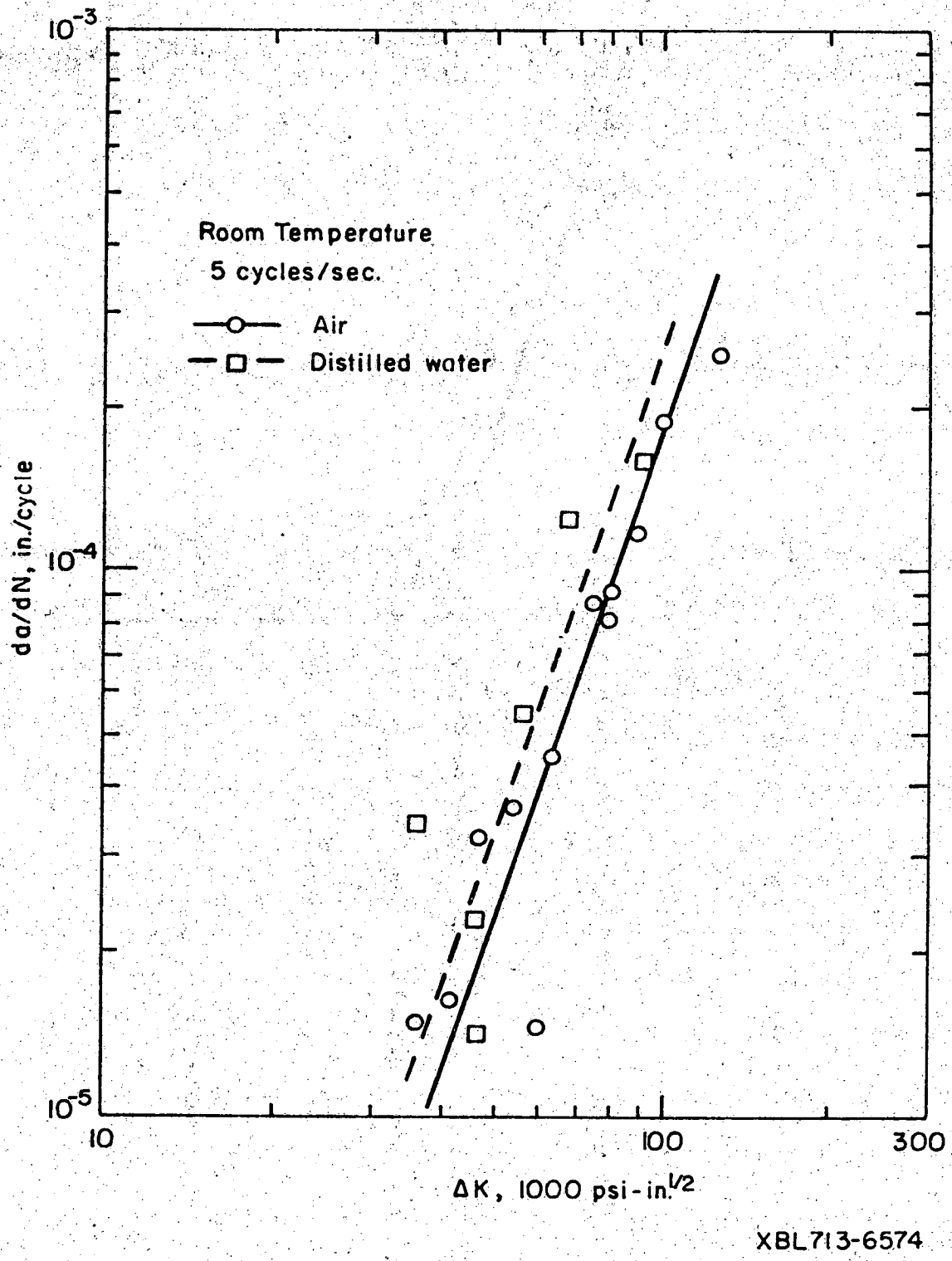
Room Temperature
5 cycles/sec.
Air
Distilled water
da/dN, in./cycle
10^{-3}
10^{-4}
10^{-5}
10
100
300
ΔK, 1000 psi-in.$^{1/2}$
XBL713-6574

Fig. 7.

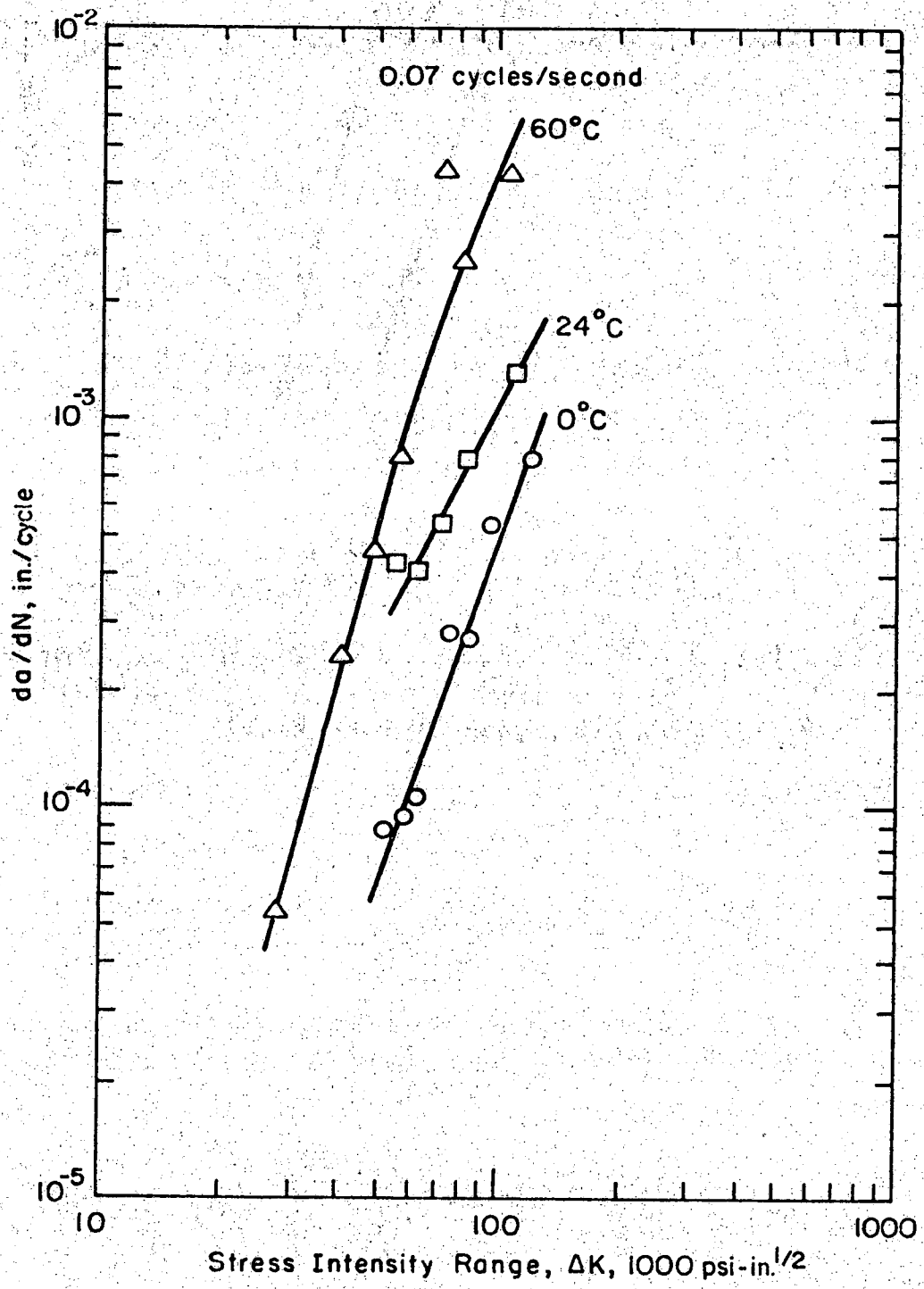

XBL713-6576

Fig. 8.

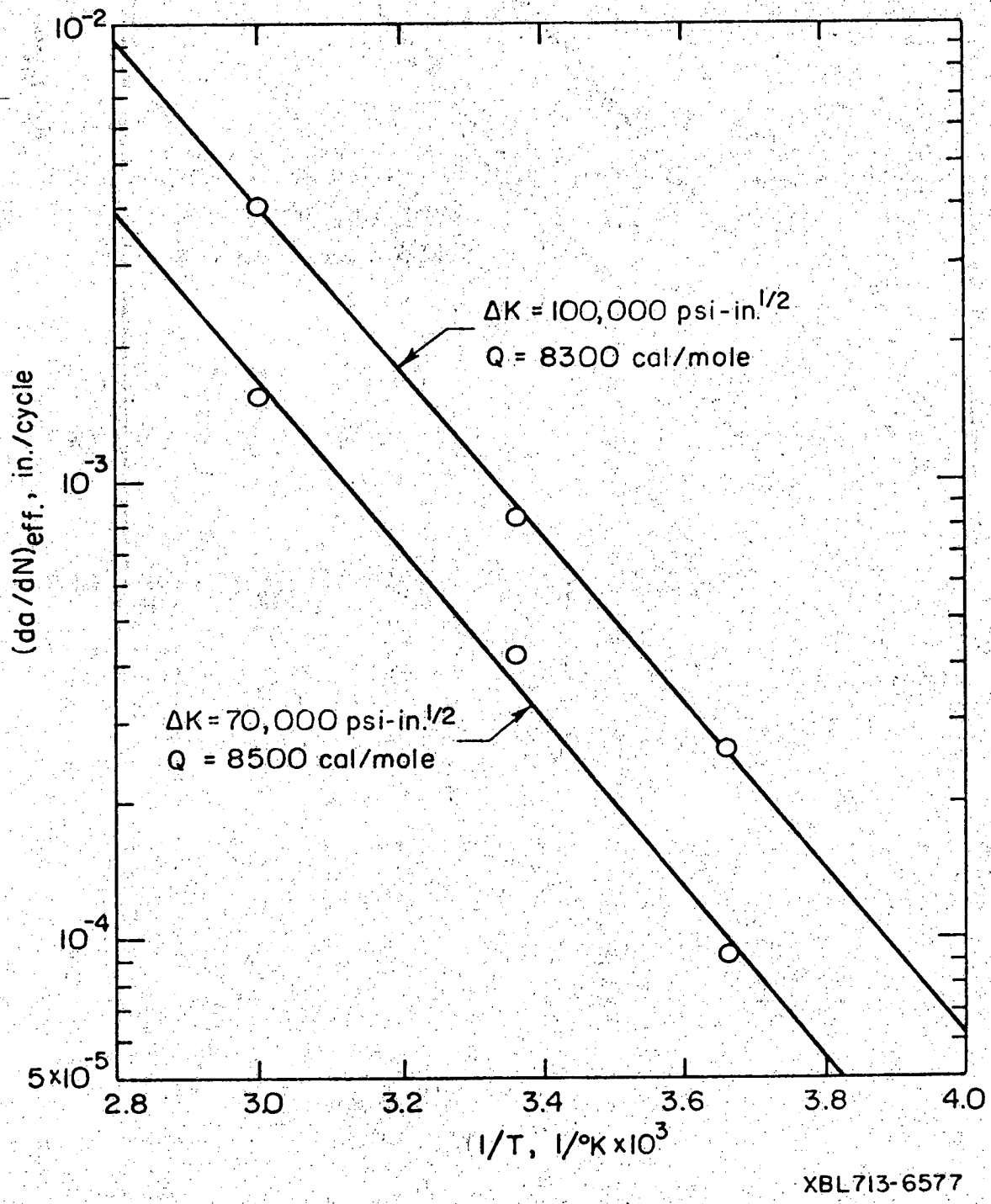
10^{-2}
10^{-3}
10^{-4}
5×10^{-5}
$(da/dN)_{eff.}$, in./cycle
ΔK = 100,000 psi-in.$^{1/2}$
Q = 8300 cal/mole
ΔK = 70,000 psi-in.$^{1/2}$
Q = 8500 cal/mole
2.8
3.0
3.2
3.4
3.6
3.8
4.0
1/T, 1/°K x10^3
XBL713-6577

Fig. 9.

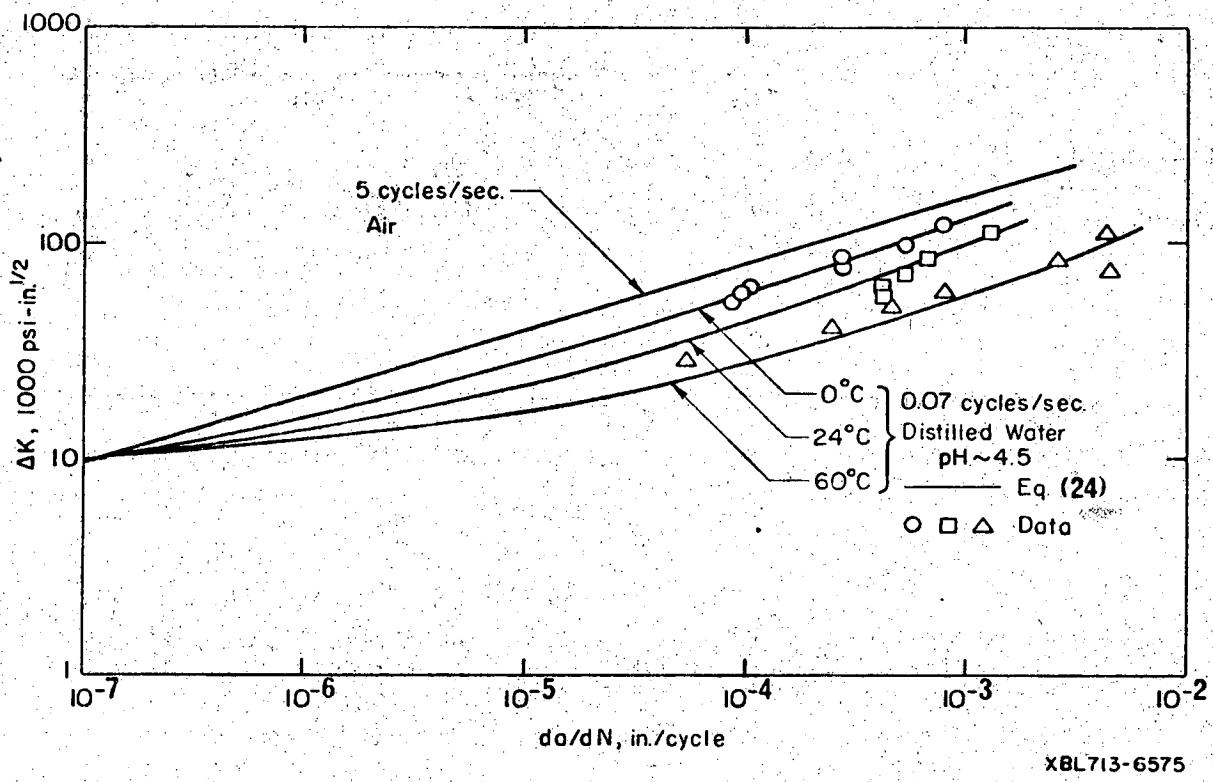
1000
100
10
1
ΔK, 1000 psi-in.$^{1/2}$
10^{-7}
10^{-6}
10^{-5}
10^{-4}
10^{-3}
10^{-2}
da/dN, in./cycle
5 cycles/sec.
Air
0°C
24°C
60°C
0.07 cycles/sec.
Distilled Water
pH~4.5
Eq. (24)
Data
XBL713-6575

Fig. 10.

LEGAL NOTICE

This report was prepared as an account of work sponsored by the United States Government. Neither the United States nor the United States Atomic Energy Commission, nor any of their employees, nor any of their contractors, subcontractors, or their employees, makes any warranty, express or implied, or assumes any legal liability or responsibility for the accuracy, completeness or usefulness of any information, apparatus, product or process disclosed, or represents that its use would not infringe privately owned rights.

TECHNICAL INFORMATION DIVISION
LAWRENCE RADIATION LABORATORY
UNIVERSITY OF CALIFORNIA
BERKELEY, CALIFORNIA 94720

DISCLAIMER

This document was prepared as an account of work sponsored by the United States Government. While this document is believed to contain correct information, neither the United States Government nor any agency thereof, nor the Regents of the University of California, nor any of their employees, makes any warranty, express or implied, or assumes any legal responsibility for the accuracy, completeness, or usefulness of any information, apparatus, product, or process disclosed, or represents that its use would not infringe privately owned rights. Reference herein to any specific commercial product, process, or service by its trade name, trademark, manufacturer, or otherwise, does not necessarily constitute or imply its endorsement, recommendation, or favoring by the United States Government or any agency thereof, or the Regents of the University of California. The views and opinions of authors expressed herein do not necessarily state or reflect those of the United States Government or any agency thereof or the Regents of the University of California.